The Effect of Biaxial Texture on the Effective Electromechanical Constants of Pollycrystalline Barium Titanate and Lead Titanate Thin Films

Jennifer L. Ruglovsky[1], Jiangyu Li[2], Kaushik Bhattacharya[1], Harry A. Atwater[1]

[1]*California Institute of Technology*
Pasadena, CA 91125

[2]*University of Washington*
Seattle, WA 98195

Keywords

piezoelectricity, thin films, texture, orientation distribution

Abstract

Effective electromechanical constants as a function of biaxial crystallographic texture in polycrystalline films are modeled using a self-consistent approach. The film is modeled by assuming Gaussian distributions of two Euler angle textures about perfect orientation with varying spread, or full width at half maximum. We see that independent in-plane texturing has little effect on the piezoelectric displacement tensor. Increased out-of-plane texturing gives rise to an enhanced piezoelectric effect for barium titanate films, but not for lead titanate. Twist texturing about these out-of-plane angles shows a further enhancement in the non-shear components of the piezoelectric displacement tensor for both materials. Finally, we use the effective piezoelectric coupling factor as the primary figure of merit for the effective piezoelectric properties of polycrystal devices, thus utilizing all electromechanical constants of this simulation. This quantity shows a primary dependence on the out-of-plane texture.

Introduction

Piezoelectric materials have long been studied for their interesting electromechanical properties. The fact that piezoelectric, elastic, and dielectric properties are coupled and switchable offers further engineering freedoms, particularly in thin films. The realization of these materials in thin film form allows for the miniaturization and integration of piezoelectric and electro-optic devices for applications in MEMs, integrated photonics, and other device technologies which can be integrated with silicon electronics.

Piezoelectric displacements and other electromechanical constants are easily quantified for single crystal materials[1,2], and the effects of rotation on these constants are also confirmed experimentally via slicing along varying orientations[3, 4]. However, most traditional thin film growth methods (CVD, Sol gel, PLD, etc.) result in polycrystalline films. In some cases, polycrystalline films can be fabricated with crystallographic microstructures that approach those of ideal single crystal materials, achieving grain orientation through epitaxial growth on lattice-matched substrates or a template layer[5]. More generally, polycrystalline films exhibit a distribution of grain orientations around a direction normal to the film plane and/or around a specific in-plane azimuthal orientation. Piezoelectric and electro-optic thin film devices typically have active regions whose dimensions are considerably larger than a single grain, and thus would be anticipated to exhibit effective properties that are characteristic of an appropriately determined ensemble response of many grains. Therefore, we consider the effect of the grain-scale mosaic spread in the crystallographic texture and orientation on the device-scale piezoelectric coupling factor achievable in thin film devices. Our method enables the effective

electromechanical properties to be obtained for a polycrystalline film. We explore tetragonal 4MM materials, and give specific results for barium titanate and lead titanate. We report here the results of self-consistent simulations of the properties of biaxially textured films, which elaborates upon work reported to date that has been only the properties of fiber-textured films.[6,7,8]

Model

The method utilized in this paper is adapted from Li's[8] consideration of effective electromechanical moduli of piezoelectric polycrystals, textured about one Euler angle (θ), with suitable modifications for incorporating a second Euler angle (ϕ or φ) for biaxially textured films. A brief summary of Li's method and our modifications is described below.

Consider a polycrystalline thin film of a ferroelectric material, and assume that the grain size is small compared to the film thickness. It is then appropriate to calculate the effective properties of bulk ceramics and then apply them to the thin film setting[9]. Each grain in the polycrystal has its own underlying domain pattern. At small and moderate applied stress and field, the domain patterns do not change and each domain responds like a piezoelectric material with its own preferred orientation. This is the medium that is considered below. Thus, texture refers to information about both the grains and domains.

The response of a piezoelectric material is described by two constitutive equations, written in Voight tensor notation[10], wherein the electric and elastic fields are fully coupled:

$$\sigma_i = C_{ij}\varepsilon_j - e_{ik}E_k,$$
$$D_l = e_{lm}\varepsilon_m + \kappa_{\ln}E_n.$$ The applied elastic stress is given by σ and the electric displacement is D. Elastic strain, ε, and electric field, E, are the field variables in the equations. The proportionality constants relating these values are C, e, and κ, which are elastic stiffness, piezoelectric stress constant, and dielectric constant, respectively. These constitutive equations may be combined in matrix representation with the following variables:

$$\Sigma = \begin{bmatrix} \sigma \\ D \end{bmatrix}, \qquad Z = \begin{bmatrix} \varepsilon \\ -E \end{bmatrix}, \qquad G = \begin{bmatrix} C & e^t \\ e & -\kappa \end{bmatrix}.$$

Thus we may consider a single constitutive equation,

$$\Sigma = GZ.$$

The effective electromechanical constants of matrix G* may be defined as

$$< \Sigma >= G^* < Z >$$

where <x> refers to a volume average of variable x,

$$< x >= \int (x) d\Omega(\theta, \varphi, \phi).$$

Li finds the G* matrix as

$$G^* =< G(\theta, \varphi, \phi) A(\theta, \varphi, \phi) >$$

where G(θ,φ,ϕ) are the electromechanical moduli of a particular grain with orientation at Euler angles θ,φ,ϕ with respect to the reference frame of sample. A(θ,φ,ϕ) is the concentration factor for a single grain with orientation at the same Euler angles θ,φ,ϕ. This factor is a function of grain shape, orientation, and interaction of neighboring grains. A proper estimation of this factor is needed to determine the effective electromechanical constants.

In the self-consistent method, the concentration factor A is determined by assuming that individual grains are embedded in an infinite matrix with yet to be determined effective moduli G*, subjected to yet to be determined external loading Z_1 at the boundary. Consider a single grain in the infinite matrix. Its response, Z, is related to the far field loading, Z_1, by:

$$Z(\theta,\varphi,\phi) = A^{dil}(\theta,\varphi,\phi)Z_1,$$

$$A^{dil}(\theta,\varphi,\phi) = \{I + S(\theta,\varphi,\phi)G^{-1}(\theta,\varphi,\phi)[G(\theta,\varphi,\phi) - G^*]\}^{-1}.$$

$A^{dil}(\theta,\varphi,\phi)$ is the solution from the problem of a single spherical inhomogeneity embedded in an infinite matrix[11]. $S(\theta,\varphi,\phi)$ is the piezoelectric Eshelby tensor for a spherical inhomogeneity at specified orientation expressed in the coordinate system of the sample. The assumption of a spherical inhomogeneity is a significant assumption since domains have a lamellar shape: however, it is reasonable for our limited purposes and easily modified. Domain configurations and their evolution are not considered, nor is phase transformation. When the applied electric field is small, this treatment is appropriate since the contribution from domain wall movement is small.

Averaging all of these individual grains' responses and insisting that this average be consistent with the applied load Z^0, we obtain[8]:

$$Z_1 = < A^{dil}(\theta,\varphi,\phi) >^{-1} Z^0 ,$$

where Z^0 is the uniform field.

Now,

$$A(\theta,\varphi,\phi) = A^{dil}(\theta,\varphi,\phi) < A^{dil}(\theta,\varphi,\phi) >^{-1},$$

and therefore the effective constants are given by:

$$G^* = < G(\theta,\varphi,\phi)(A^{dil}(\theta,\varphi,\phi) >< A^{dil}(\theta,\varphi,\phi) >^{-1}.$$

This self-consistent approach has G* on both sides of the equation, so the solution must be found numerically by iteration.

Clearly, the numerical solution requires volume averages. The distribution of grains is introduced as an Orientation Distribution Function (ODF), W, which is the orientational probability density function for each grain. Volume averages for an aggregate collection of such grains are then determined as follows:

$$< H >= \int_0^{2\pi}\int_0^{2\pi}\int_{-1}^{1} H(\cos\theta,\varphi,\phi) W(\cos\theta,\varphi,\phi) d\cos\theta d\varphi d\phi$$

where $H(\cos\theta,\varphi,\phi)$ is the single crystal value with reference to the grain's location in the sample. Our determination of G* above has such a volume average for both $G(\theta,\varphi,\phi)A^{dil}$ and A^{dil}. The

integrals for each are solved by Gaussian quadratures, wherein the integral of a function is approximated by the sum of its function values at a set of points called abscissas, multiplied by weighting coefficients.

The aggregate grains are assumed to have a Gaussian distribution. For biaxial texture, we use two combinations of angles for two separate ODFs, W_1 and W_2:

$$W_1(\theta,\varphi,\phi) = \frac{1}{\alpha\sqrt{2\pi}}\frac{1}{\beta\sqrt{2\pi}}Exp(-\frac{\theta^2}{2\alpha^2})Exp(-\frac{\phi^2}{2\beta^2}),$$

$$W_2(\theta,\varphi,\phi) = \frac{1}{\alpha\sqrt{2\pi}}\frac{1}{\gamma\sqrt{2\pi}}Exp(-\frac{\theta^2}{2\alpha^2})Exp(-\frac{\varphi^2}{2\gamma^2}).$$

The parameters α, βandγ are increasing figures of merit to describe worsening texture for Euler angles θ, ϕ, and φ, respectively. As α, β, $\gamma \rightarrow 0$, we approach perfectly aligned grains which are thus indistinguishable from single crystals, and as α, β, $\gamma \rightarrow \infty$ we approach a randomly oriented, non-piezoelectric film. In both ODFs, the angle that does not appear (φ for W_1 and ϕ for W_2) is assumed to be randomly distributed within the film.

Recently Brewer et al.[12] devised a Reflection High Energy Electron Diffraction (RHEED) -based analysis technique to determine quantitative full width at half maximums (FWHMs) of in- and out-of-plane texture angles for the piezoelectric films based on diffraction patterns and changes with rocking curve measurements. Consequently, the parameters α and β in the above ODF W_1 can be directly compared to the FWHM of θ and ϕ given from the RHEED experiment. Thus effective properties of a collection of grains in a device may be correlated with experimental

observations of biaxial texture. Narrow distributions approaching single crystal texture have been realized with measured FWHM θ around 3^o and FWHM ϕ around 7^o. The second case of biaxial texture, depending on parameters α and γ, would be more difficult to measure experimentally, as the Euler angle φ is only measured once the grain has been displaced by Euler angle θ. Nevertheless, one could imagine a rocking curve scheme where the out-of-plane angle θ was situated, and an entire rocking curve for an in-plane angle about that θ was obtained, giving the texture about φ, with respect to the original sample reference frame.

The results of this simulation are three-dimensional surfaces of effective constants (e, C, and κ) with input α and βorγ, herein referred to as FWHM θ, FWHM ϕ and FWHM φ.

Results

The theory described above is applied to barium titanate and lead titanate polycrystals. Both of these perovskite materials exhibit 4MM symmetry, but the single crystal piezoelectric constants of each differ significantly, as seen in Table 1. This difference contributes to the extent of the effect of texture on each material's electromechanical properties.

A. Piezoelectric strain constant

As piezoelectric devices are often characterized by piezoelectric strain coefficient d, defined as $d_{ij}=\varepsilon_i/E_j$, we begin the analysis with this electromechanical constant. The constitutive equations given above rely on the e value, or piezoelectric stress constant. This tensor is easily converted to d by normalizing with C, the stiffness tensor.

A1. Biaxial Texture with mosaic spread about ϕ and θ

Biaxial texture with mosaic spread about the ϕ and θ Euler angles is analogous to a thin film polycrystal with in- and out-of-plane texturing, rotating the z (out-of-plane) and x and y-axes (in-plane) independently. Results for d tensor components (only d_{31}, d_{33}, and d_{15} are non-zero in 4MM symmetry) for both barium titanate and lead titanate (at FWHM □=0 cross-section) are shown in Fig. 1. Consistent with Li's results[8] for a fiber-textured polycrystal, we see that for barium titanate, values d_{31} and d_{33} show an increase from single crystal values with some critical texturing about Euler angle θ. However, this enhancement is not seen in lead titanate.

The difference between barium titanate and lead titanate can be attributed to the single crystal piezoelectric displacement tensor values for each tetragonal material. Consider the effect of rotation on the single crystal value d_{zz} measured at an angle θ with respect to the [001] direction:

$$d_{zz} = d_{33}\cos^3\theta + (d_{15}+d_{31})\cos\theta \sin^2\theta.$$

This is displayed in Fig. 2. We see that barium titanate actually has a higher d_{zz} at some angular rotation θ away from the [001]. The maximum d_{zz} is at $\theta=52^o$, close to the [111] orientation. The highest value for lead titanate, on the other hand, exactly coincides with the [001] direction. Thus the effect of rotating barium titanate grains with respect to the applied field will therefore increase its effective piezoelectric constants, whereas those of lead titanate will decrease monotonically. We also therefore remark that a polycrystalline barium titanate film with [111] texture would have a higher effective piezoelectric displacement d_{zz} than a [001] textured polycrystal.

The single crystal plots of the piezoelectric constant for each material in Fig. 2 also give us insight into the effects on piezoelectric displacement from texturing about Euler angle ϕ, or in-plane texturing. For both barium and lead titanate, the single crystal plots above have azimuthal symmetry. Thus we expect very little effect on the effective piezoelectric constant via variation of in-plane texture. We have found that this is indeed the case. The FWHM ϕ=0 curve is shown in Fig. 1. However, there is a slight effect of in-plane spread in barium titanate's effective d_{33} constant, depicted in Fig. 3, and a mirrored enhancement in the effective d_{31} value (not shown). Since the piezoelectric tensor transformations are independent of ϕ, [Appendix 1] we conclude that the slight enhancement must be due to the intergranular constraints, brought out from the self-consistent simulation.

Finally, the results for d_{31}, d_{33}, and d_{15} for both materials show that with increasing FWHM θ (indicating a degradation of fiber texture to a completely random polycrystal), all the effective piezoelectric constants asymptote to 0, indicating the polycrystal has become non-piezoelectric, as expected.

A2. Biaxial Texture with mosaic spread about φ and θ

The second case of biaxial texture considered is one which allows each grain to rotate about the Euler angles θ and φ. This corresponds to a film with grains possessing some out-of-plane rotation from a z-axis, perpendicular to the plane of the film, and some in-plane rotation about the newly rotated axis.

In Fig. 4, at low FWHM φ there is a pronounced variation in d_{33} and d_{31} in barium titanate, and a slighter variation for the same components of lead titanate. There is very little effect of spread in φ for the d_{15} component (data not shown). It does seem reasonable that a lower 'twist' φ about each out-of-plane angle θ would give rise to higher values of piezoelectric displacement, as tetragonal grains would be well-oriented in the normal plane to the new out-of-plane axis, and that the shear component d_{15} would not be as sensitive to this twist. Shown also is the dependence on both angles from the single crystal rotation matrices with transformations depending on θ and φ. The piezoelectric tensor depends on both angles, unlike the rotation about θ and ϕ, which only depends on θ [Appendix 2]. Finally we remark about the asymptotes. As FWHM θ increases, the piezoelectric constants asymptote to those of a random and non-piezoelectric polycrystal, with piezoelectric constants equal to 0, and as FWHM φ increases, we generate an identical curve to the d values of the previous section, as φ becomes randomly distributed.

B. Piezoelectric coupling factor

As a final component of our analysis and discussion, we perform analysis in terms of a meaningful figure of merit for piezoelectric performance in polycrystalline film-based devices. Traditionally, piezoelectric displacement has been used as a figure of merit, hence the detailed analysis above. However if the application required a more detailed prediction of device performance, incorporating robustness of the film and support of fields, we would instead chose the primary figure of merit for performance of polycrystalline thin film devices, the piezoelectric coupling factor, k, defined as the stored mechanical energy per unit input electrical energy:[14]

$$k = \frac{d^2 C}{\hat{e}^o \hat{e}}$$

From our model, the effective piezoelectric displacement, elastic stiffness, and the dielectric constant tensors may be combined in a meaningful way to yield this single, dimensionless value.

B1. Biaxial Texture with mosaic spread about ϕ and θ

Below are the results k_{31}, k_{33}, and k_{15} for biaxially textured films about θ and ϕ of both barium and lead titanate. We find that the results are independent of ϕ. The variation with FWHM θ is shown in Fig. 5. The constants decrease monotonically and asymptote to zero. We see that once again the azimuthal symmetry of the piezoelectric displacement components results in little effect of in-plane texture. We recall that barium titanate showed an increase in d_{33} and d_{31} with texture about θ, but encorporating stiffness and the dielectric constant with texture for the k values, we do not see an enhancement in coupling factor for barium titanate, only a decrease.

B2. Biaxial Texture with mosaic spread about φ and θ

For biaxially textured film rotated about θ and φ, we see slight dependence on FWHM φ. Fig. 6 shows envelopes of data at FWHM φ=0 and FWHM φ=∞. A narrow distribution about perfect alignment does enhance the coupling factors for both materials in all 3 tensor values around FWHM θ in the range of 0.1 to 1. With a larger distribution, indicating a random texture of Euler angle φ, we see the identical curves as in Fig. 5, as expected. Even with the profound enhancement in d_{33} and d_{31} with an effective collection of grains with low twist angle φ about each θ (Fig. 4), the coupling factor follows a gradual decreasing trend.

Conclusion and Discussion

A self-consistent approach was used to model effective electromechanical constants as a function of biaxial texture in polycrystalline films of barium and lead titanate. In-plane texturing has little effect on any of the electromechanical constants. Out-of-plane texturing increases the effective piezoelectric strain constants for barium titanate, but not for lead titanate. With biaxial texturing out-of-plane and twisting about each angle, we see large enhancements in piezoelectric constants. Finally, considering the effective piezoelectric coupling factor for these materials, we see a primary dependence on the out-of-plane texture.

Given the ultimate goal in researching thin film ferroelectric materials is the fabrication and optimization of devices, we must pay attention to the coupling factor results of this model, which incorporate all of the film's effective electromechanical constants. For a given sample geometry and electrode configuration, we would choose a given k component to give information about the device performance. For instance, k_{15} would be used to analyze a sample with interdigitated electrodes, and k_{33} or k_{31} for blanket electrodes, given a tent or cantilever geometry, respectively.

As seen above, biaxially textured films (about either set of angles) present no great advantage to fiber textured films when the coupling factor is used as a figure of merit. Thus devices fabricated with traditional growth methods for observation of the direct piezoelectric effect may be optimized by minimizing the texture about Euler angle θ, or out-of-plane distribution.

Acknowledgements

This work was supported by the United States Department of Defense MURI award DAAD19-01-1-0517, administered by the Army Research Office and Arrowhead Research Corporation.

References

[1] D. Berlincourt and H. Jaffe, *Phys. Rev. B* Vol 111, No. 1, pp. 143-8 (1958).

[2] Z. Li, M. Grimsditch, C. M. Foster, and S-K. Chan, *J. Phys. Chem Solids* Vol 57, No. 10, pp. 1433-8 (1996).

[3] X. Du, Q. Wang, U. Belegundu, A. Bhalla, and K. Uchino, *Materials Letters* 40, pp. 109-13 (1999).

[4] C. Harnagea, A. Pignolet, M. Alexe, and D. Hesse, *Integrated Ferroelectrics* 44, pp. 113-24 (2002).

[5] R.T. Brewer, H.A. Atwater, J.R. Groves, and P.N. Arendt, *J. Appl. Phys.* 93 (1), pp. 205-10 (2003).

[6] J.Y. Li, M.L. Dunn, and H. Ledbetter, *J. Appl. Phys.* 86, pp. 4626-34 (1999).

[7] Y.C. Zhou, J. Liu, and J.Y. Li, *Appl. Phys. Lett.* 86, 262909 (2005).

[8] J.Y. Li, *J. Mech. Phys. Solids* 48, pp. 529-52 (2000).

[9] Y.C. Shu, *Arch. Rat. Mech. Anal.* 153, pp. 39-90 (2000).

[10] J.F. Nye, *Physical Properties of Crystals*, Oxford University Press 1957.

[11] M.L. Dunn and M. Taya, *Proc.R. Soc. Lond. A,* Vol. 443, pp. 265-287 (1993).

[12] R.T. Brewer, D.A. Boyd, M.Y. El-Naggar, S.W. Boland, Y.B. Park, S.M. Haile, D.G. Goodwin, and H.A. Atwater, *J. Appl. Phys.* 97(3), 034103 (2005).

[13] M. Zgonik, P. Bernasconi, M. Duelli, R. Schlesser, P. Gunter, M. Garrett, D. Rytz, Y. Zhu, and X. Wu, *Phys. Rev. B.* 50, pp. 5941-9 (1994).

[14] K.Uchino, *Ferroelectric Devics*, Marcel Dekker, Inc. 2000.

Table 1. Material constants for barium titanate (BTO)[13] and lead titanate (PTO)[2] single crystals.

	C_{11}(GPa)	C_{12}(GPa)	C_{13}(GPa)	C_{33}(GPa)	C_{44}(GPa)	C_{66}(GPa)
BTO	222	108	111	151	61	134
PTO	235	101	98.8	105	65.1	104

	e_{31}(C/m^2)	e_{33}(C/m^2)	e_{15}(C/m^2)	κ_{11}/κ_0	κ_{33}/κ_0
BTO	-0.7	6.7	34.2	2200	56
PTO	-0.98	3.35	3.92	80	34

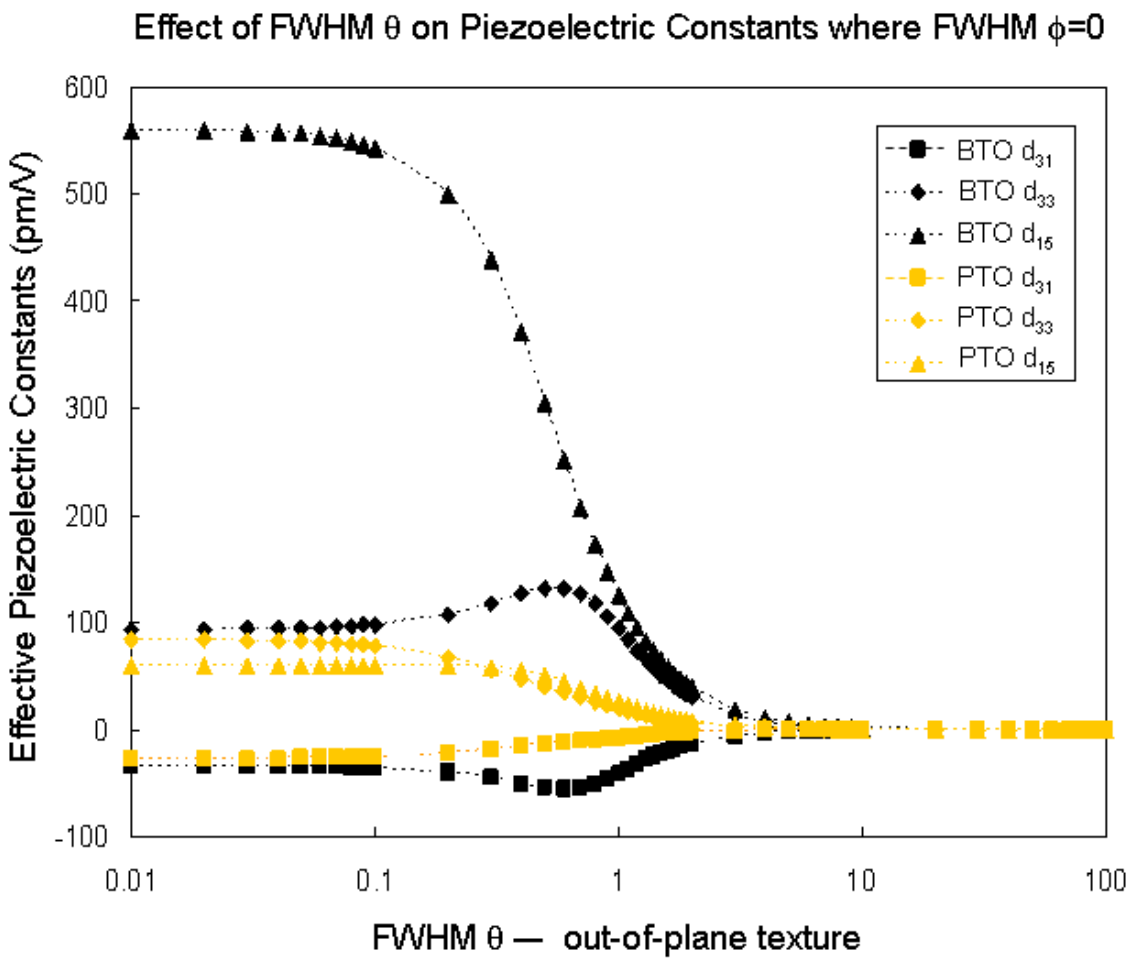

Figure 1. Variation of effective piezoelectric displacements d_{31}, d_{33}, and d_{15} with the FWHM of the out-of-plane texture distribution for textured barium titanate (BTO) and lead titanate (PTO) polycrystalline films (FWHM ϕ=0).

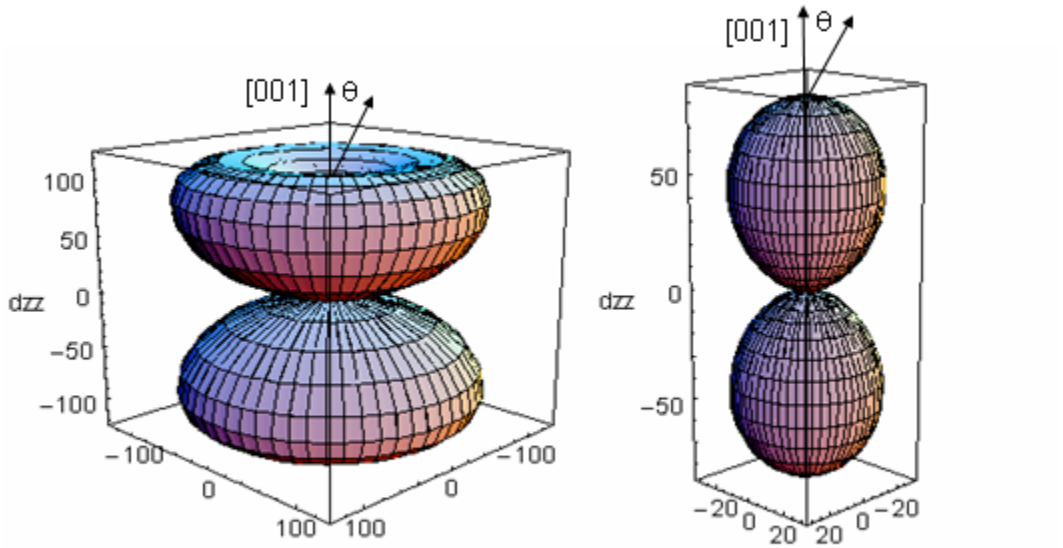

2(a) Barium Titanate 2(b) Lead Titanate

Figure 2. Variation of perpendicular piezoelectric displacement d_{zz}, with polar angle θ, under applied perpendicular E-field.

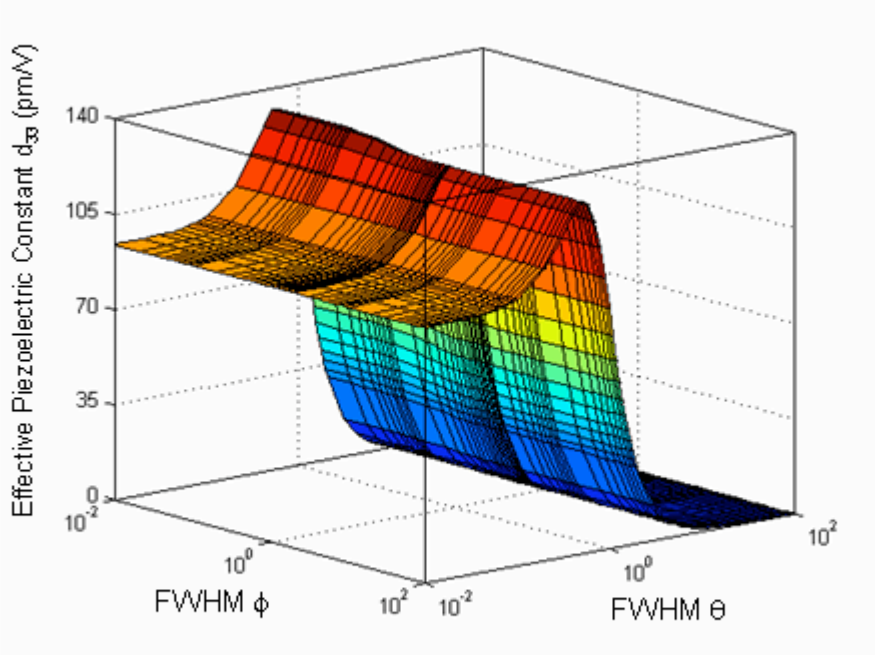

Figure 3. Variation of effective piezoelectric displacements d_{33} with the FWHM of the in- and out-of-plane texture distribution for a textured barium titanate polycrystalline film.

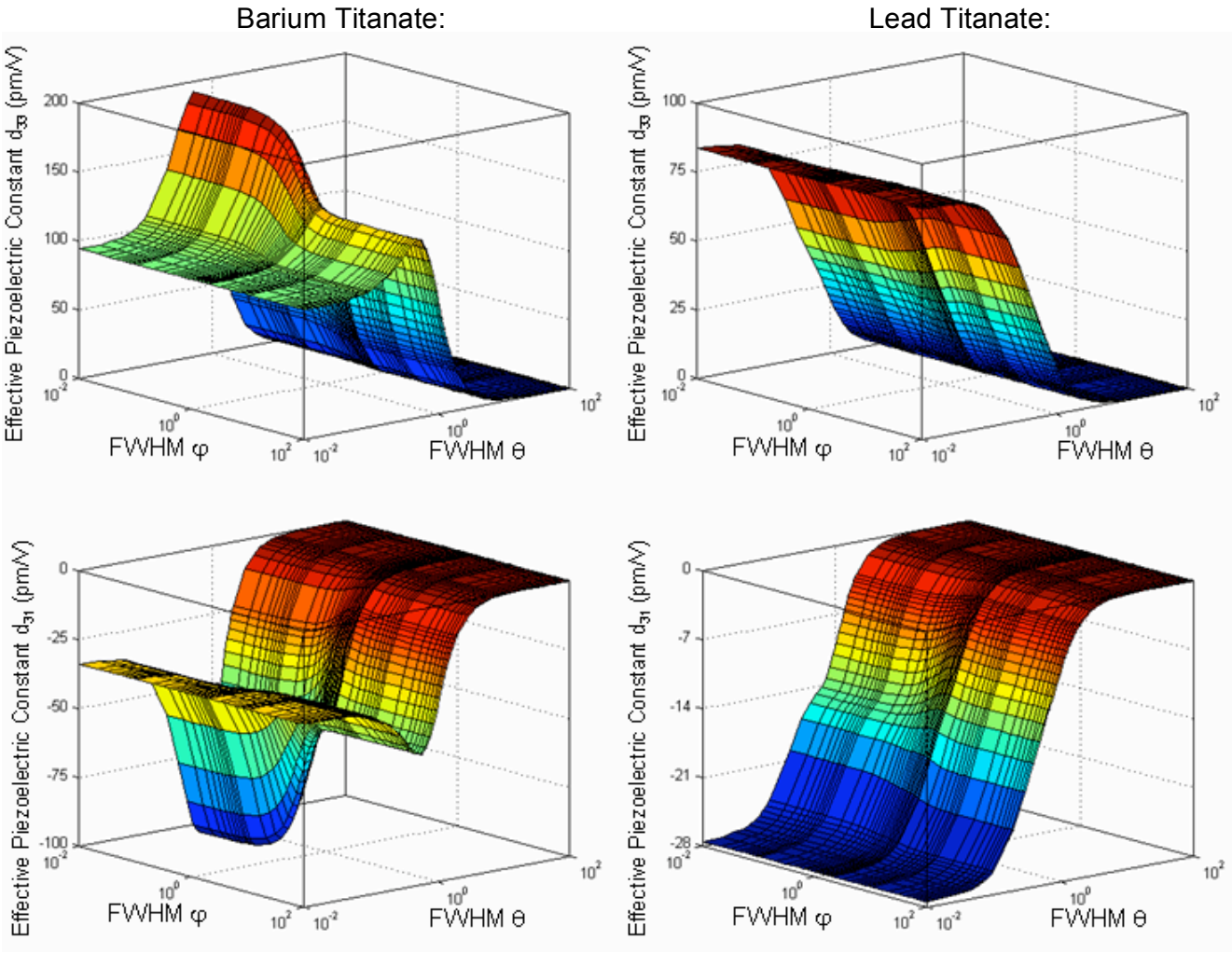

Figure 4. Variation of effective piezoelectric displacements d_{33} and d_{31} with the FWHM of the out-of-plane and twisted texture distribution for textured barium titanate and lead titanate polycrystalline films.

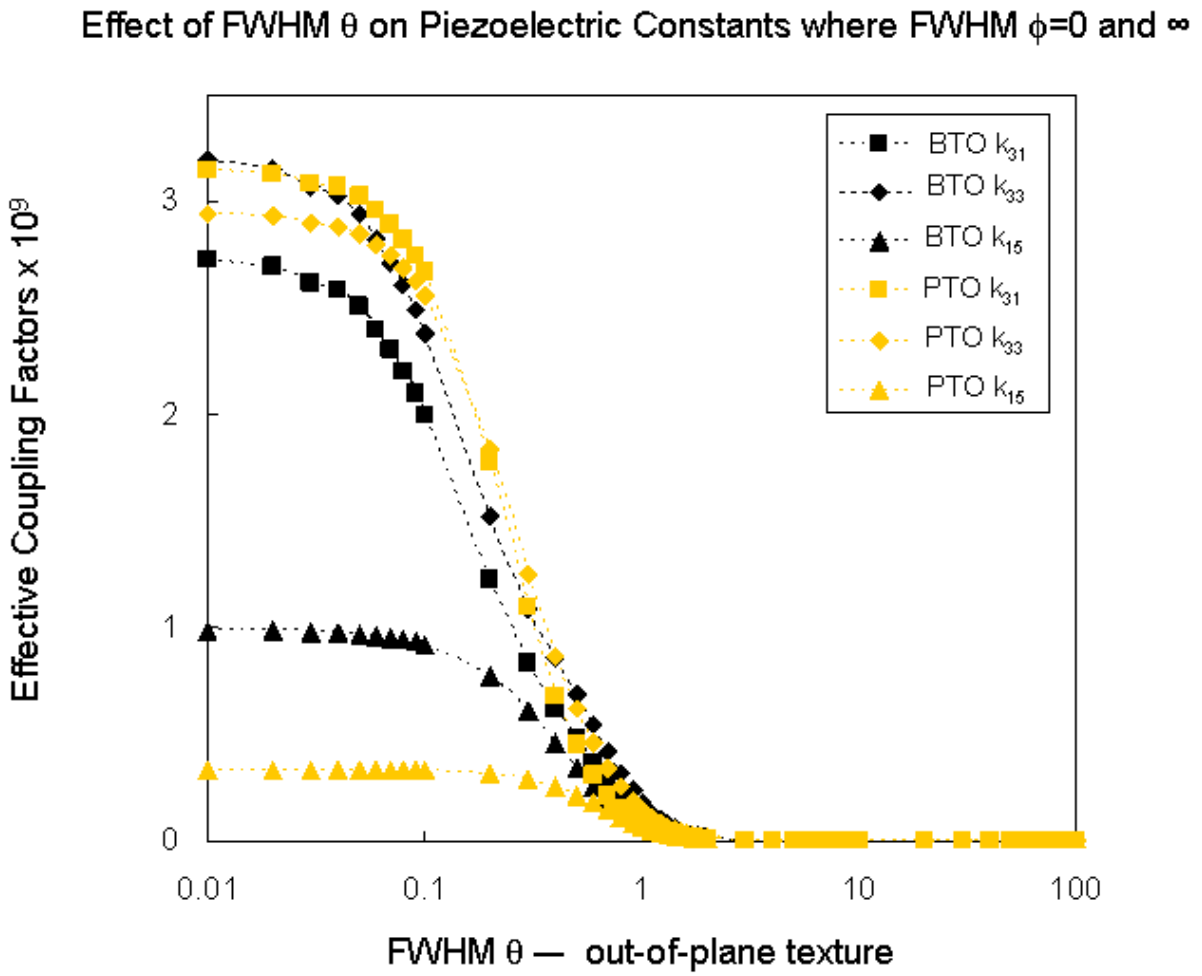

Figure 5. Variation of effective piezoelectric coupling factors k_{31}, k_{33}, and k_{15} with the FWHM of the out-of-plane texture distribution for textured barium titanate (BTO) and lead titanate (PTO) polycrystalline films (FWHM ϕ= 0 and ∞).

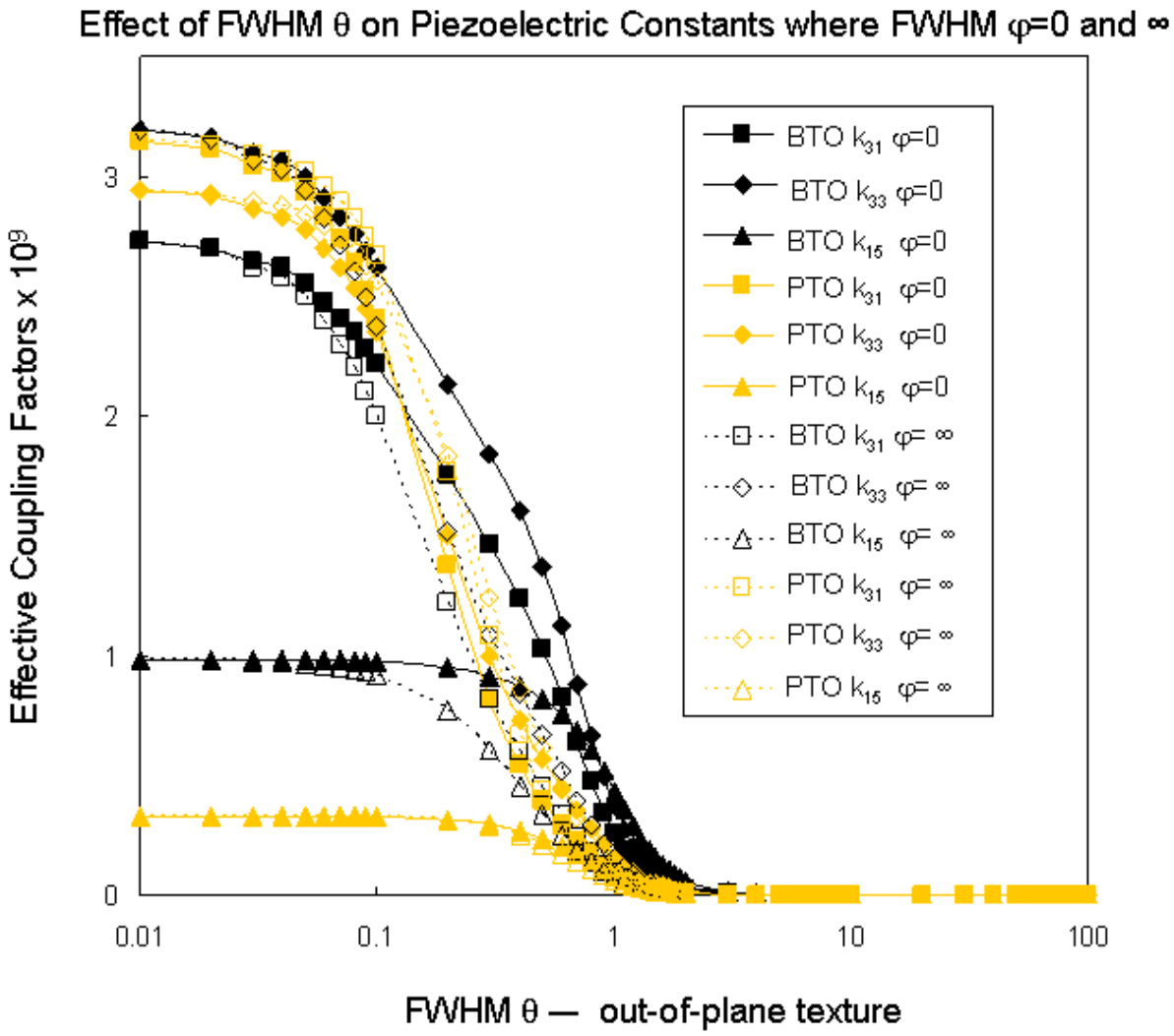

Figure 6. Variation of effective piezoelectric coupling factors k_{31}, k_{33}, and k_{15} with the FWHM of the out-of-plane texture distribution at FWHM of the twist distribution at 0 and ∞ for textured barium titanate (BTO) and lead titanate (PTO) polycrystalline films.

Appendix 1.
3x6 tensor for d rotated with ϕ and θ.

Column 1

0
$d_{31}\sin\theta$
$d_{31}\cos\theta$

Column 2

0
$\frac{1}{2}\sin\theta\,[d_{15}+d_{31}+d_{33}+(d_{15}+d_{31}-d_{33})\cos 2\theta]$
$\frac{1}{2}\cos\theta\,[-d_{15}+d_{31}+d_{33}+(d_{15}+d_{31}-d_{33})\cos 2\theta]$

Column 3

0
$-\frac{1}{2}\sin\theta\,[d_{15}-d_{31}-d_{33}+(d_{15}+d_{31}-d_{33})\cos 2\theta]$
$\frac{1}{2}\cos\theta\,[d_{15}+d_{31}+d_{33}-(d_{15}+d_{31}-d_{33})\cos 2\theta]$

Column 4

0
$\frac{1}{2}\cos\theta\,[-d_{31}+d_{33}+(d_{15}+d_{31}-d_{33})\cos 2\theta]$
$-\frac{1}{2}\sin\theta\,[d_{31}-d_{33}+(d_{15}+d_{31}-d_{33})\cos 2\theta]$

Column 5

$\frac{1}{2}\,d_{15}\cos\theta$
0
0

Column 6

$\frac{1}{2}\,d_{15}\sin\theta$
0
0

Appendix 2.
3x6 tensor for d rotated with θ and φ.

Column 1

$\sin\varphi\ \sin\theta\ (d_{15}+d_{31})(\cos^2\varphi+\cos^2\theta\sin^2\varphi)+d_{33}\sin^3\varphi\ \sin^3\theta$
$\cos\varphi\ \sin\theta\ [d_{31}\cos^2\varphi+\sin^2\varphi(-d_{15}+(d_{15}+d_{31})\cos^2\theta+d_{33}\sin^2\theta)]$
$\cos\theta\ [d_{31}\cos^2\varphi+\sin^2\varphi(d_{31}\cos^2\theta+(-d_{15}+d_{33})\sin^2\theta)]$

Column 2

$\sin\varphi\ \sin\theta\ [d_{31}\sin^2\varphi+\cos^2\varphi(-d_{15}+(d_{15}+d_{31})\cos^2\theta+d_{33}\sin^2\theta)]$
$\cos\varphi\ \sin\theta\ (d_{15}+d_{31})(\cos^2\varphi\ \cos^2\theta+\sin^2\varphi)+d_{33}\cos^3\varphi\sin^3\theta$
$\cos\theta\ [d_{31}\sin^2\varphi+\cos^2\varphi(d_{31}\cos^2\theta+(-d_{15}+d_{33})\sin^2\theta)]$

Column 3

$\sin\varphi\ \sin\theta\ [(-d_{15}+d_{33})\cos^2\theta+d_{31}\sin^2\theta]$
$\cos\varphi\ \sin\theta\ [(-d_{15}+d_{33})\cos^2\theta+d_{31}\sin^2\theta]$
$d_{33}\cos^3\theta+(d_{15}+d_{31})\cos\theta\sin^2\theta$

Column 4

$-(d_{15}+d_{31}-d_{33})\cos\varphi\ \cos\theta\ \sin\varphi\ \sin^2\theta$
$\frac{1}{2}\ \cos\theta\ [\cos^2\varphi(-d_{31}+d_{33}+(d_{15}+d_{31}-d_{33})\cos2\theta)+d_{15}\sin^2\varphi]$
$-\frac{1}{2}\ \cos\varphi\ \sin\theta\ [d_{31}-d_{33}+(d_{15}+d_{31}-d_{33})\cos2\theta]$

Column 5

$\frac{1}{2}\ \cos\theta\ [d_{15}\cos^2\varphi+(-d_{31}+d_{33}+(d_{15}+d_{31}-d_{33})\cos2\theta)\ \sin^2\varphi]$
$-(d_{15}+d_{31}-d_{33})\cos\varphi\ \cos\theta\ \sin\varphi\ \sin^2\theta$
$-\frac{1}{2}\ \sin\varphi\ \sin\theta\ [d_{31}-d_{33}+(d_{15}+d_{31}-d_{33})\cos2\theta]$

Column 6

$\frac{1}{2}\ \cos\varphi\ \sin\theta\ [d_{15}\cos^2\varphi+(-d_{31}+d_{33}+(d_{15}+d_{31}-d_{33})\cos2\theta\sin^2\varphi]$
$\frac{1}{2}\ \sin\varphi\ \sin\theta\ [\cos^2\varphi(-d_{31}+d_{33}+(d_{15}+d_{31}-d_{33})\cos2\theta)+d_{15}\sin^2\varphi]$
$-(d_{15}+d_{31}-d_{33})\cos\varphi\ \cos\theta\ \sin\varphi\ \sin^2\theta$